TISSUE ENGINEERING: Part C
Volume 19, Number 4, 2013
© Mary Ann Liebert, Inc.
DOI: 10.1089/ten.tec.2011.0745

Zero Echo Time Magnetic Resonance Imaging of Contrast-Agent-Enhanced Calcium Phosphate Bone Defect Fillers

Yi Sun, MSc,[1,2,*] Manuela Ventura, MSc,[3,*] Egbert Oosterwijk, PhD,[2]
John A. Jansen, DDS, PhD,[3] X. Frank Walboomers, PhD,[3] and Arend Heerschap, PhD[1]

Calcium phosphate cements (CPCs) are widely used bone substitutes. However, CPCs have similar radiopacity as natural bone, rendering them difficult to be differentiated in classical X-ray and computed tomography imaging. As conventional magnetic resonance imaging (MRI) of bone is cumbersome, due to low water content and very short T_2 relaxation time, ultra-short echo time (UTE) and zero echo time (ZTE) MRI have been explored for bone visualization. This study examined the possibility to differentiate bone and CPC by MRI. T_1 and T_2* values determined with UTE MRI showed little difference between bone and CPC; hence, these materials were difficult to separate based on T_1 or T_2 alone. Incorporation of ultra-small particles of iron oxide and gadopentetatedimeglumine (Gd-DTPA; 1 weight percentage [wt%] and 5 wt% respectively) into CPC resulted in visualization of CPC with decreased intensity on ZTE images in *in vitro* and *ex vivo* experiments. However, these additions had unfavorable effects on the solidification time and/or mechanical properties of the CPC, with the exception of 1% Gd-DTPA alone. Therefore, we tested this material in an *in vivo* experiment. The contrast of CPC was enhanced at an early stage postimplantation, and was significantly reduced in the 8 weeks thereafter. This indicates that ZTE imaging with Gd-DTPA as a contrast agent could be a valid radiation-free method to visualize CPC degradation and bone regeneration in preclinical experiments.

Introduction

To heal bone tissue loss and damage, autologous grafting remains the preferred clinical option. However, autograft material is scarce and thus the implantation of synthetic bone grafts at the site of injury is sometimes necessary.[1] Among a large number of available bone substitutes, calcium phosphate cement (CPC) best resembles the matrix of natural bone. The high similarity of CPC to natural bone not only promotes bone regeneration, but also results in low contrast between CPC and native bone tissue in X-ray and computed tomography (CT) imaging. Therefore, it remains difficult to monitor the degradation of the cements and regeneration of bone tissue, hampering the evaluation of repair procedures. A strategy to overcome this problem is the addition of contrast agents to CPC. For example, contrast agents with iodine, barium, and tantalum have been utilized in X-ray to increase radiopacity of CPCs, which allowed discriminating them from bone tissue.[2–5] X-ray imaging provides adequate resolution with high throughput at low cost, but with relatively poor contrast and potential radiation damage.[6]

Magnetic resonance imaging (MRI) is a noninvasive, radiation-free, high-resolution technique, which however is mostly optimized to visualize soft tissues. The MR signals are generated from the proton spins in water molecules, if placed in a strong magnetic field, by a radiofrequency (RF) pulse. In an explorative animal study, it was shown that MRI could be a valuable tool in bone tissue engineering.[7] However, due to a relatively low content of water protons and their ultra-short T_2 relaxation (e.g., cortical bone has a mean T_2 value of 500 μs or less[8]), MRI of rigid tissue and solid material is still challenging. Some approaches that have been proposed to image hard tissues are solid-state and single-point MR techniques,[9,10] but these are unfavorable for *in vivo* applications due to long acquisition times. Following improvements in hardware and MR methods, an echo time of less than hundreds of μs could be reached by ultra-short echo time (UTE) imaging either employing a short nonselective RF excitation pulse with 3D radial sampling or using a two half-pulse free induction decay (FID) acquisition.[11,12] Suppression of long-T_2 spins from soft tissue have further improved and extended this technique and its derivatives.[13,14] More recently, a no-echo-time method called sweep imaging with

Departments of [1]Radiology, [2]Urology, and [3]Biomaterials, Radboud University Nijmegen Medical Centre, Nijmegen, The Netherlands.
*Both authors equally contributed to this work.

Fourier transformation (SWIFT) was introduced, which acquires data quasi-simultaneously with the excitation pulse, using adiabatic pulses. It already has been applied in imaging of bone samples and thermoplastic objects.[15, 16] Another approach without echo time spin evolution is zero echo time (ZTE) MR.[17–20] It is closely related to UTE and has been implemented on small animal MR systems.[21] A hard RF pulse is applied to accomplish spatially nonselective excitation that covers the full frequency bandwidth spanned by the readout gradient. Excitation and acquisition is both in the presence of a constant gradient purely used for frequency encoding by 3D radial center-out k-space trajectories. Thus, these recently developed MR methods offer new options to image bone and might also be applicable to examine bone filler material.

The aim of this study was to explore bone and CPC imaging by the ZTE method, and to evaluate the incorporation of two clinical MRI contrast agents, ultra-small particles of iron oxide (USPIO) and gadopentetatedimeglumine (Gd-DTPA). This included the determination of useful contrast levels for *in vivo* experiments, the characterization of changes in the properties of CPC after addition of contrast agents, the measurement of T_1 and T_2* relaxation times of materials and surrounding bone, and finally monitoring the substitutes' degradation in an *in vivo* experiment.

Materials and Methods

Injectable CPC preparation and contrast agents incorporation

CPC consisted of 85% α-tricalcium phosphate, 10% dicalcium phosphate dihydrate, and 5% hydroxyapatite. The liquid applied to make cement was a sterilized 2 weight percentage (wt%) aqueous solution of sodium phosphate (Na_2HPO_4). Poly(lactic-co-glycolic acid) particles (PLGA, Purasorbs; Purac, Gorinchem, the Netherlands) with a lactic-to-glycolic-acid ratio of 50:50 was used for microparticle preparation.[22] PLGA was mixed with the cement powder at 20 wt% to create microporosity. The mixture was sterilized using gamma radiation with 25 KGy (Isotron B.V., Ede, the Netherlands). After adding a filtered sterilized (0.2 μm filter) 2% aqueous solution of Na_2HPO_4 to the PLGA/CPC powder, the mixture was put into a 2-mL syringe (BD Plastipak; Becton Dickinson S.A., Madrid, Spain) with a closed tip. These components were shaken for 20 s with a mixing apparatus (Silamat, Vivadent, Schaan, Liechtenstein) to generate injectable CPC. For the incorporation of USPIO (Sinerem®), it was directly added to the liquid Na_2HPO_4 solution with cement before mixing. From a USPIO solution of 21 mg/mL, 120 and 600 μL were applied for 1 wt% and 5 wt% USPIO-CPC respectively. Gd-DTPA particles (MagneVist®) were incorporated within the cement powder after freeze drying; 6 and 30 μL were taken from a solution of 469 mg/mL to make 1 wt% and 5 wt% Gd-DTPA-CPC respectively.

CPC characterization

The solidification times measurement and compression tests to examine clinical handling proprieties of the CPC were performed as follows:

Setting time is the time required to reach a certain compressive strength.[23] Initial and final setting time of different formulations were assessed by using custom available Gillmore needles (ASTM C266). Preset scaffolds at a size of 3 mm (diameter) × 6 mm (height) were made from a plastic mould. Samples from each formulation were mixed and injected into the mould, and then both initial and final setting times were determined. Tests were performed at room temperature.

For compression tests, samples were placed in a testing bench (858 MiniBionixII®; MTS, Eden Prairie, MN) and compressive strength and E-modulus in the longitudinal direction (parallel to the long axis) of the specimens were measured at 0.5 mm/min crosshead speed.

For both tests, data are presented as mean ± standard deviation. Significant differences were determined by analysis of variance. Calculations were performed using GraphPad-Instat® (GraphPad Software, San Diego, CA). All differences were considered significant at p-values < 0.05.

In vitro *and* ex vivo *test of CPC repaired bone*

For *in vitro* tests bone blocks of 1.5 cm^3 were harvested from pig bone. A cylindrical defect of 3 mm in depth and diameter was drilled using a dental bur and dental drills. Defects were then filled with injectable CPC. The filler material was tested with contrast agent (USPIO or Gd-DTPA) in different concentrations (1% and 5%) for each formulation. CPC without contrast agents were applied as control. Photos of bone blocks were taken, and then the MR images were acquired.

The feasibility to use USPIO as contrast agent for localization of bone filler was also tested on a rat cadaver. A cylindrical defect of 3 mm depth and diameter was drilled in the femoral condyle, and subsequently this defect was repaired with CPC containing 1 wt% USPIO.

In vivo *animal model*

National guidelines for care and use of laboratory animals were obeyed with approval of the Experimental Animal Ethical Committee of the University Medical Center Nijmegen (RU-DEC 2010-225). In two healthy adult male Wistar rats, weighing 250–300 g, femoral condyle defects were created. The first rat had a defect in one leg repaired by CPC and one healthy leg, while the second rat had a defect in one leg repaired with Gd-DTPA-CPC and a defect on the other leg left unrepaired. The Gd-DTPA concentration was 1 wt% of the cement powder. Surgery was performed under general inhalation anesthesia (Isoflurane) and sterile conditions. Animals were immobilized and legs were shaved, washed, and disinfected before surgery. The knee joint became totally exposed after a longitudinal parapatellar incision. At the femoral intercondylar notch a cylindrical defect of 3.0 mm depth and diameter was prepared using a dental bur and continuous external cooling with saline. Defects were then filled with proper material or left unrepaired before closing.

T_1 and T_2 measurement using UTE*

The UTE sequence (see Fig. 1 for basic pulse sequence) was applied to measure T_1 (spin-lattice relaxations time) and T_2* (relaxation due to spin–spin interactions and field inhomogeneities), of two bone samples (harvested from the rat leg) with defects that had been repaired with CPC and Gd-DTPA-CPC respectively.

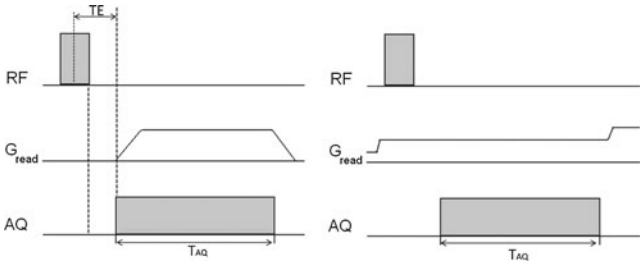

FIG. 1. Left: 3D ultra-short echo time (UTE) sequence, 3D radial sampling applied after nonselective radiofrequency (RF) excitation pulse, TE min = t pulse/2 + delay. Delay is the time to switch from transmit to receive mode. Right: zero echo time (ZTE) pulse sequence, excitation, and acquisition are both in the presence of constant gradient, with an effective echo time of zero.

The standard parameters were: TR = 8 ms, FOV = 30 × 30 × 30 mm, matrix size: 128 × 128 × 128, and 8 averages.

To measure T_2* values, several images were obtained with different echo times. As femoral head and CPCs bone fillers have extremely short T_2* relaxation time, echo times were mostly chosen in the initial signal decay part after the 5° excitation pulse, that is, at 40, 60, 80, 100, 200, 400, 600, 800, and 1000 μs.

Assuming a mono-exponential decay the signal intensity (S_{TE}) is related to the echo time (TE) according to the equation[24,25]:

$$S_{TE} = S_0 \times e^{-TE/T2^*} + C$$

S_0 is the initial value of signal intensity and C is the background noise. By fitting this equation to the experimental data, the T_2* relaxation time was calculated.

For T_1 measurements, the variable flip angle method[26] was applied. The steady state signal achieved when TR > > T_2*, result in the following equation for signal intensity:

$$S\alpha = \frac{NM_0 e^{-TE/T2} * \sin\alpha(1 - e^{-TR/T1})}{1 - \cos\alpha(e^{-TR/T1})}$$

N represents a constant, M_0 is the net magnetization at thermal equilibrium, and α is the flip angle. This equation can be rearranged:

$$S_\alpha / \sin\alpha = e^{-TR/T1} S_\alpha / \tan\alpha + NM_0 e^{-Te/T2^*}(1 - e^{-TR/T1})$$

Linear regression is independent of N, T_2*, and TE allowing the calculation of T_1. By using variable flip angles (α = 2.5°, 5°, 7.5°, 10°, and 12.5°), TE = 0.04 ms, and other standard parameters in UTE, images with signal intensity as a function of T_1 were obtained.

Regions of interests were manually outlined on the bone filler and about the same number of pixels on femoral head using Paravision 5.1(Bruker, Biospin, Germany). Average signal intensities of a selected region on UTE images were calculated using the same program, and then processed in GraphPad Prism® (GraphPad Software).

MR imaging

MRI of bone samples was performed on an 11.7T MR system (Biospec, Bruker, Germany) with a home-built Helmholtz coil, with a size of 3 × 3 cm. The standard ZTE imaging (pulse sequence diagram is shown in Fig. 1) was done with 200 kHz bandwidth, pulse length = 0.002 ms, TR = 4 ms, FOV = 50 × 50 × 50 mm, matrix size: 128 × 128 × 128, 1 average, and a total acquisition time of 3 min 27 s. Conventional MRI of bone was acquired with 3D RARE, with FOV = 50 × 50 × 50 mm, TE/TR = 35.7 ms/1000 ms, RARE factor = 16, and acquisition time of 8 min 32 s. ZTE imaging of cadaver rats were performed on the same MR system and using the same acquisition parameters.

For *in vivo* experiments, ZTE imaging was done right after surgery and 8 weeks postoperation on 2 animals with similar parameters as in the standard acquisition protocol, but with TR = 8 ms, 4 averages, and a total acquisition time around 30 min. Because of the use of a ZTE sequence, other rigid materials such as the animal bed and holders, water heating system, and RF coil housing may give background signal. Therefore, proton-free materials were applied wherever possible.

In vivo *CT imaging*

For comparison with MRI, the nondefect leg was imaged on a small animal scanner (Inveon®; Siemens Preclinical Solutions, Knoxville, TN). Scans were performed under general inhalation anesthesia (Isoflurane). The animal was placed in a supine position in the scanner and images were acquired over ~6 min (spatial resolution 30.04 μm, 80 kV, and 500 μA; exposure time 1000 ms; and frame average by 1). CT values of air (−1000 HU) and water (0 HU) were applied to calibrate the image values in Hounsfield units, while the bone mineral density values provided a linear calibration for bone mineral density values. CT images were reconstructed using a modified cone-beam algorithm.[27]

Results

CPC characterization

For CPC doped with USPIO at concentrations of 1 wt% and 5 wt%, the initial and final setting times were substantially prolonged compared with normal CPC (Table 1). For the formulations with 1 wt% and 5 wt% Gd-DTPA no significant change in final setting times compared with normal CPC was observed. Compression tests of CPC with 5% Gd-DPTA and 5% USPIO showed a significant decrease of the peak load (Table 1). In contrast, adding 1% Gd-DPTA and 1% USPIO did not result in a significant change. In

Table 1. Setting Time and Compression Test

Gillmore test & compression test	*Initial setting time (min)*	*Final setting time (min)*	*Peak load (N)*
CPC	8.9 ± 0.53	22.0 ± 0.42	31.9 ± 5.05
Gd-DTPA 1%	12.4 ± 0.55	21.4 ± 0.42	32.0 ± 13.61
Gd-DTPA 5%	15.4 ± 0.34	27.3 ± 0.22	5.74 ± 0.39
USPIO 1%	50.8 ± 3.09	114.5 ± 3.14	35.3 ± 21.77
USPIO 5%	140.4 ± 9.34	21.3 ± 0.83	17.1 ± 8.02

To determine the setting time a standard Gillmore test was used, initial needle diameter 1/12 inch, Weight ¼ lb; Final needle diameter 1/24 inch, Weight ¼ lb.

CPC, calcium phosphate cement; USPIO, ultra-small particles of iron oxide; Gd-DTPA gadopentetatedimeglumine.

conclusion, the setting time and the mechanical properties of CPC were not affected by adding 1% Gd-DTPA.

In vitro *and* ex vivo *imaging of repaired bone*

Visual inspection of pig bone blocks repaired with pure CPC revealed a white lesion with a sharp edge, making the cement easily discernible from bone (Fig. 2A). In MR images there was little contrast between bone and CPC, even in images obtained by ZTE (Fig. 2E). For the Gd-DTPA incorporated CPCs filler, visual inspection showed the same contrast as for pure CPC (Fig. 2B), but with enhanced contrast in ZTE imaging (Fig. 2F). Finally, with USPIO incorporation the lesion became black (Fig. 2C, D) and showed large effects on ZTE images, due to the so-called "blooming effect" of the iron oxide particles (Fig. 2G, H).

To test the feasibility of applying USPIO as a contrast agent in animal experiments, an *ex vivo* experiment was performed on bone defect repaired by 1 wt% USPIO tagged CPCs, since the lower concentration had less effect on the properties of CPC. On conventional MRI, bone and normal CPC both appear dark (Fig. 3A), with little bone detail. In contrast, bone structure is clearly seen on the ZTE images (Fig. 3B). However, the strong blooming effect rendered the precise localization of USPIO-CPC filler cumbersome, also in ZTE imaging (Fig. 3B).

T_1 and T_2 measurement of bone and bone fillers*

Using 3D UTE at different echo times T_2* relaxation times were assessed. The signal decay in these measurements were fitted with a mono-exponential function (see Fig. 4), resulting in T_2* relaxation times of 597 ± 19 μs for bone, 442 ± 22 μs for CPC, and 226 ± 18 μs for Gd-DTPA-CPCs.

For the T_1 measurements the variable flip angle method was used. This resulted in T_1 relaxation time of 474.19 ± 28 ms for bone, 527 ± 29 ms for CPC, and 336.44 ± 25 ms for Gd-DTPA loaded CPCs. Thus T_1 and T_2* values were both shortened due to Gd-DTPA incorporation.

In vivo *imaging of CPC repaired femoral condyle defects*

On ZTE images of the rat leg without defect, bone and surrounding tissues were clearly distinguishable (Fig. 5A). Despite that, the resolution of the image of rat condyle measured by ZTE MRI was lower than those obtained by CT (Fig. 5B). It has sufficient image quality to provide complementary structural diagnostic information on bone and surrounding soft tissue like muscles and meniscus.

For *in vivo* assessment of contrast enhancement in ZTE imaging of repaired bone lesions we selected CPC doped with 1% Gd-DTPA, as this formulation had similar mechanical properties as normal CPC (without Gd-DTPA). Lesions filled with the contrast agent loaded CPC showed a decreased signal intensity compared with the surrounding bone tissue (Fig. 6A, B), reflecting the shortened relaxation times. The shape and location of the filler material were clearly visible. This contrast decreased after 8 weeks, but it was still possible to differentiate the lesion location from bone (Fig. 6C).

Lesions filled with normal CPC showed little contrast with bone on ZTE images immediately postoperation. This contrast was further degraded 8 weeks later, so that the lesion was virtually invisible (Fig. 6D, E).

Discussion

In this study we demonstrated that bone defects repaired by CPC could be distinguished from surrounding bone on MR images by using a ZTE sequence and mixing the CPC with a contrast agent. Among the contrast formulations

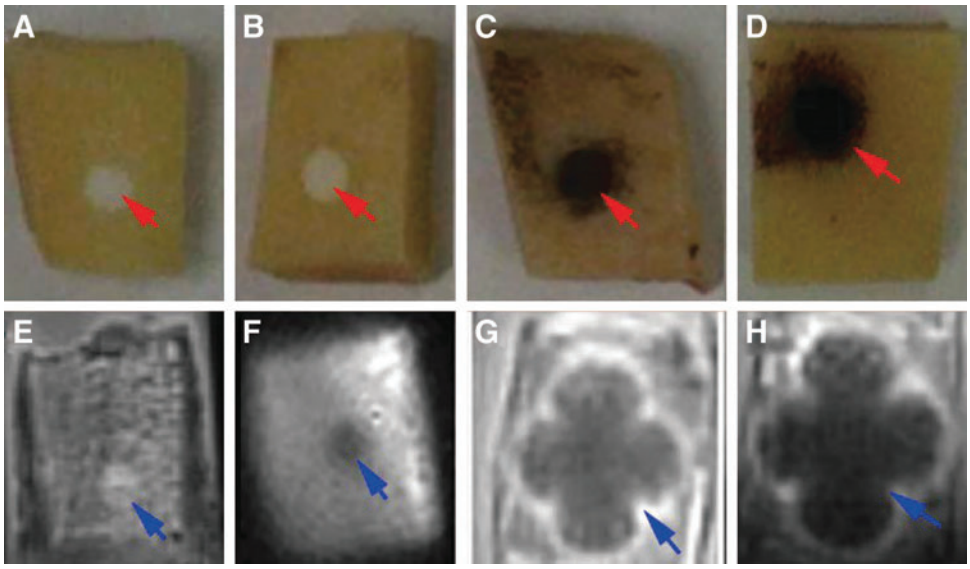

FIG. 2. Macroscopic views and magnetic resonance (MR) images of bone samples with defect in bone blocks repaired by calcium phosphate cement (CPCs). The lesions with bone filler material are indicated by red arrows in the pictures **(A–D)** and by blue arrows in the magnetic resonance imaging (MRI), which were obtained by ZTE imaging **(E–H)**. **(A, E)** No contrast agent; **(B, F)** with gadopentetatedimeglumine (Gd-DTPA) 1wt%; **(C, G)** with ultra-small particles of iron oxide (USPIO) 1 wt%; **(D, H)** with USPIO 5 wt%; note the stronger blooming effect with 5 wt% USPIO **(H)**. Color images available online at www.liebertpub.com/tec

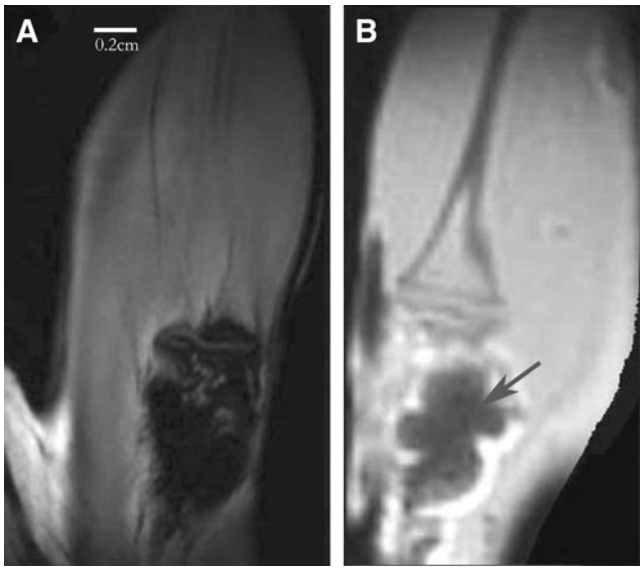

FIG. 3. *Ex vivo* MR images of 2 rat legs with repaired defects. **(A)** Bone and CPC appear dark and no detail is apparent in conventional MRI (3D RARE). **(B)** ZTE image of the bone defect repaired by USPIO CPC, bone details, and lesion site can be discerned. Note the strong blooming effect (arrow).

tested the clinical approved Gd-DTPA at 1 wt% appeared to be most practical. This would enable the evaluation of bone regeneration in studies to optimize procedures for lesion repair.

CT has been used in the past in the imaging of repaired bone lesions. To distinguish bone defects filled with CPC from surrounding tissue this also requires a contrast enhancer (radiopacifier), such as tantalumpentoxide.[28] Especially in longitudinal CT studies the accumulation of radiation becomes a matter of concern.[6] Therefore, MRI has

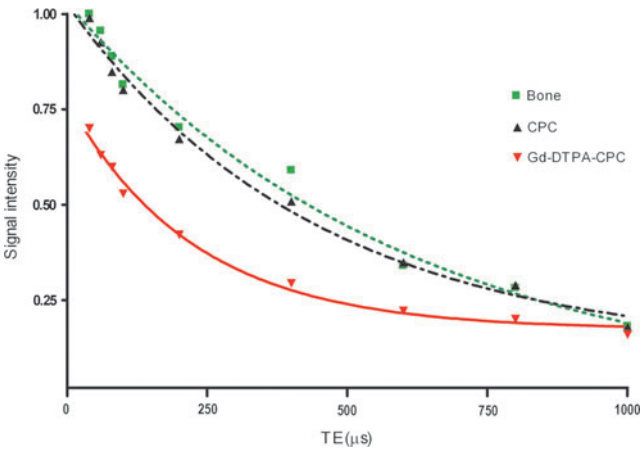

FIG. 4. Signal intensity plotted versus TE in UTE acquisition of bone and CPC materials. All curves are normalized to 100% signal intensity at the first measurement point of bone. Dashed and dotted line (black): fit of T2* decay of CPC. Dotted line (green): fit of bone T2* decay. Red line: fit of T2* decay of 1 wt% Gd-DTPA loaded CPC. Color images available online at www.liebertpub.com/tec

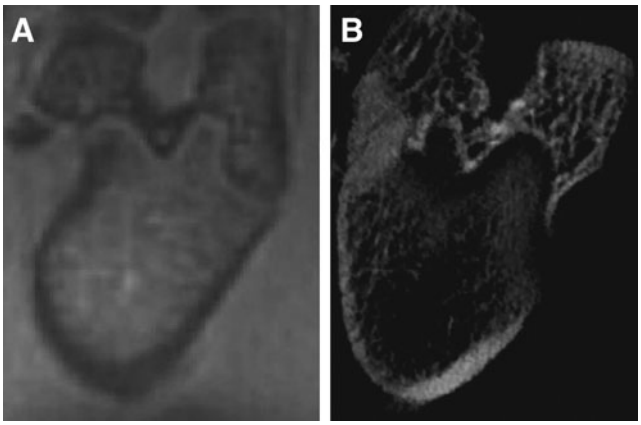

FIG. 5. **(A)** ZTE image of healthy rat condyle, soft tissues like muscles are surrounding the bone structure. **(B)** *In vivo* computed tomography of the same body part.

attracted attention as an alternative in the imaging of bone and hard tissue. For example, T_1-weighted MRI on bone implants with gadolinium-based contrast clearly demonstrated the potential of MRI to study bone formation[29] and gadoteratemeglumine was developed to enhance MRI of bone cement.[30] However, none of these experiments yet demonstrated *in-vivo* MRI of the material. Further, as only conventional MRI was used signal intensity was not optimal.

Since both bone and CPC have very short T_2 values (< 1 ms), it is problematic to visualize these materials with conventional MRI, as signal rapidly disappears in the echo times of several ms or more. A UTE sequence provides the possibility to obtain MR images at echo time below 1 ms,[12] but this sequence has some intrinsic problems, like errors from eddy-currents generated by the gradient ramps, which need to be corrected by k-space trajectory measurements; additionally, the ramp reduces the signal to noise ratio.[21] Therefore, the use of ZTE imaging, which samples signal without an echo time delay, was explored to visualize bone and CPC at optimal signal strength. In this study, it was shown that with ZTE indeed good images of bone and CPC could be obtained. And a comparison with CT shows that interesting complementary information of bone may be obtained. In practice, both UTE and ZTE suffer from dominating signals of long T_2 spin systems, in particular of soft tissue,[31] and optimally need a long T_2 suppression element in the pulse sequence to reduce this problem. An advantage of the UTE sequence is its flexibility, which allows to filter out signals of species with extremely short T_2* values if needed (e.g., background signal from coil housing).

The similar T_1 and T_2* values of bone and CPC preclude their discrimination by ZTE MRI based on relaxation properties alone. Therefore, the additions of Gd-DTPA and USPIO as MR contrast agents to CPC were explored. By far, the strongest effects was seen with USPIO, but the region occupied by the filler was heavily overestimated due to blooming effects, which made precise localization of the defect difficult. This is also expected to interfere with the proper quantitative assessment of CPC degeneration and bone regeneration by ZTE imaging. Another problem with USPIO addition was the detrimental effect on the solidification time and mechanical properties of the CPC. By lowering the iron

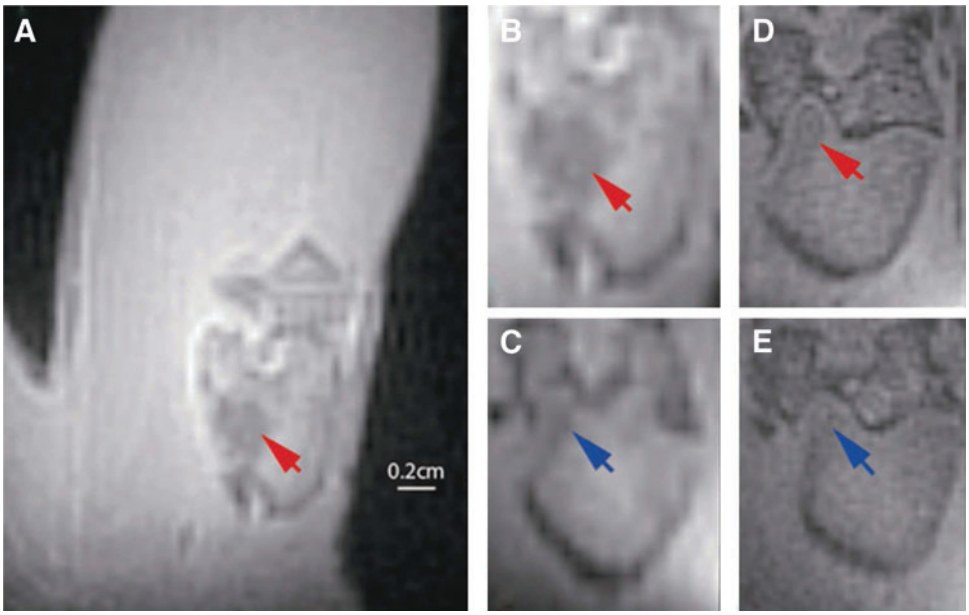

FIG. 6. *In vivo* ZTE MR images of femoral condyle defects in rat leg. **(A)** Femor with bone defect filled with Gd-DTPA-CPC. **(B)** Zoomed part of image in **(A)**, only showing the femoral condyle. **(D)** Same condyle, 8 weeks after the first scan **(B)**. **(C)** Condyle from another rat, with defect filled with CPC without contrast added. **(E)** Same condyle 8 weeks after first scan **(C)**. Arrows indicate position of lesion with CPC+1% Gd-DTPA (red) and CPC without contrast agent (blue). Color images available online at www.liebertpub.com/tec

concentration and using alternate types of iron oxide-based contrast agent with less susceptibility effects, it might be possible to minimize both the blooming problem and the detrimental effects on CPC properties and meet the requirements for *in vivo* use. For the other contrast agent tested in this study, Gd-DTPA, a decrease in mechanical strength and setting times at a concentration of 5% was also observed, but not at 1%. Therefore, the addition of 1 wt% Gd-DTPA to CPC was selected for testing *in vivo* and it was demonstrated that this enhanced the MR visibility of lesions repaired with CPC in the time immediately postoperation. The lower signal intensity reflects a shorter T_2* of CPC. Contrast became less after 8 weeks; likely because of CPC degradation, resulting in loss and dilution of the contrast agent. This was proven by histology as will be demonstrated in a separate article.

The use of gadolinium in contrast agents is associated with the risk of nephrogenic systemic fibrosis.[32] The commonly applied dose of Gd-DTPA in the clinic is 0.1 mmol/kg (0.2 mL/kg).[33] In this study, the amount we injected was 6 μL (in Gd-DTPA-CPC), which results in less than 0.03 mL/kg in the rat body. Locally, Gd-DTPA in CPC will be at relatively high concentration and slowly released in the body.

In the future, with fine-tuning of contrast agent formulations, more optimal MR acquisition parameter values and suppression of long T_2 signals are expected to further improve the contrast between bone and CPC. Also, the usage of iron oxide contrast at low dose is an option, especially if the signal intensity change can be correlated with its concentration.[34] In principle also other MR approaches have potential to visualize repaired bone lesions like the use of ^{19}F nuclei in contrast material[35] or the application of ^{31}P MR to differentiate between natural and synthetic hydroxyapatite.[36]

In conclusion, this study reported on the first *in vivo* MRI of a CPC repaired lesion in bone, using a ZTE acquisition sequence and clinically approved Gd-DTPA for enhanced contrast. This offers a novel radiation-free method to visualize CPC degradation and bone regeneration in preclinical experiments.

Acknowledgments

The authors would like to thank Mark van Uden and Andor Veltien for their support with hardware maintenance. The research leading to these results has received funding from the European Community's Seventh Framework Programme (MultiTERM, grant agreement No. 238551) and from an NWO investment grant (No. 40-00506-98-06021).

Disclosure Statement

No competing financial interests exist.

References

1. Salgado, A.J., Coutinho, O.P., and Reis, R.L. Bone tissue engineering: state of the art and future trends. Macromol Biosci **4,** 743, 2004.
2. Chan, D.C., Titus, H.W., Chung, K.H., Dixon, H., Wellinghoff, S.T., and Rawls, H.R. Radiopacity of tantalum oxide nanoparticle filled resins. Dental Mater **15,** 219, 1999.
3. Leng, Y.X., Chen, J.Y., Yang, P., Sun, H., Wang, J., and Huang, N. The biocompatibility of the tantalum and tantalum oxide films synthesized by pulse metal vacuum arc source deposition. Nucl Instr Meth Phys Res B **242,** 30, 2006.
4. Schulz, H., Mädler, L., Pratsinis, S.E., Burtscher, P., and Moszner, N. Transparent nanocomposites of radiopaque, flame-made Ta_2O_5/SiO_2 particles in an acrylic matrix. Adv Funct Mater **15,** 830, 2005.
5. Zitter, H., and Plenk, H., Jr. The electrochemical behavior of metallic implant materials as an indicator of their biocompatibility. J Biomed Mater Res **21,** 881, 1987.
6. Badea, C.T., Drangova, M., Holdsworth, D.W., and Johnson, G.A. In vivo small animal imaging using micro-CT and digital subtraction angiography. Phys Med Biol **53,** 319, 2008.
7. Hartman, E.M., Pikkemaat, J., Vehof, J.M., Heerschap, A., Jansen, J., and Spauwen, P.M. *In vivo* magnetic resonance imaging explorative study of ectopic bone formation in the rat. Tissue Eng **8,** 1029, 2002.

8. Robson, M., Gatehouse, P.D., Bydder, M., and Bydder, G. Magnetic resonance: an introduction to ultrashort TE (UTE) imaging. J Comput Assist Tomogr **27,** 825, 2003.
9. Baumann, M.A., Doll, G.M., and Zick, K. Stray-field imaging (STRAFI) of teeth. Oral Surg Oral Med Oral Pathol **75,** 517, 1993.
10. Gruwel, M., Latta, P., Tanasiewicz, M., Volotovskyy, V., Sramek, M., and Tomanek, M. MR imaging of teeth using a silent single point imaging technique. Appl Phys A Mater Sci Process **88,** 763, 2007.
11. Gatehouse, P.D., and Bydder, G.M. Magnetic resonance imaging of short T2 components in tissues. Clin Radiol **58,** 1, 2003.
12. Tyler, D.J., Robson, M.D., Henkelman, R.M., Young, I.R., and Bydder, G.M. Magnetic resonance imaging with ultrashort TE (UTE) PULSE sequences: technical considerations. J Magn Reson Imaging **25,** 279, 2007.
13. Larson, P.E., Gurney, P.T., Nayak, K., Gold, G.E., Pauly, J.M., and Nishimura, D.G. Designing long-T_2 suppression pulses for ultrashort echo time imaging. Magn Reson Med **56,** 94, 2006.
14. Du, J., Hamilton, G., Takahashi, A., Bydder, M., and Chung, C.B. Ultrashort echo time spectroscopic imaging (UTESI) of cortical bone. Magn Reson Med **58,** 1001, 2007.
15. Garwood, M., and DelaBarre, L. The return of the frequency sweep: designing adiabatic pulses for contemporary NMR. J Magn Reson **153,** 155, 2001.
16. Idiyatullin, D., Corum, C., Park, J.Y., and Garwood, M. Fast and quiet MRI using a swept radiofrequency. J Magn Reson **181,** 342, 2006.
17. Hafner, S. Fast imaging in liquids and solids with the backprojection low angle shot (BLAST) technique. Magn Reson Imaging **12,** 1047, 1994.
18. Madio, D.P., and Lowe, I.J. Ultra-fast imaging using low flip angles and FIDs. Magn Reson Med **34,** 525, 1995.
19. Kuethe, D.O., Adolphi, N.L., and Fukushima, E. Short data-acquisition times improve projection images of lung tissue. Magn Reson Med **57,** 1058, 2007.
20. Wu, Y., Ackerman, J.L., Chesler, D.A., Li, J., Neer, R.M., Wang, J., and Glimcher, M.J. Evaluation of bone mineral density using three-dimensional solid state phosphorus-31 NMR projection imaging. Calcif Tissue Int **62,** 512, 1998.
21. Weiger, M., Pruessmann, K.P., and Hennel, F. MRI with zero echo time: hard versus sweep pulse excitation. Magn Reson Med **66,** 379, 2011.
22. Habraken, W.J., Wolke, J.G., Mikos, A.G., and Jansen, J.A. Injectable PLGA microsphere/calcium phosphate cements: physical properties and degradation characteristics. J Biomater Sci Polym Ed. **17,** 1057, 2006.
23. Bohner, M. Reactivity of calcium phosphate cements. J Mater Chem **17,** 3980, 2007.
24. Du, J., Carl, M., Bydder, M., Takahashi, A., Chung, C.B., and Bydder, G.M. Qualitative and quantitative ultrashort echo time (UTE) imaging of cortical bone. J Magn Reson **207,** 304, 2010.
25. Springer, F., Martirosian, P., Schwenzer, N.F., Szimtenings, M., Kreisler, P., Claussen, C.D., and Schick, F. Three-dimensional ultrashort echo time imaging of solid polymers on a 3-Tesla whole-body MRI scanner. Invest Radiol **43,** 802, 2008.
26. Fram, E.K., Herfkens, R.J., Johnson, G.A., Glover, G.H., Karis, J.P., Shimakawa, A., Perkins, T.G., and Pelc, N.J. Rapid calculation of T1 using variable flip angle gradient refocused imaging. Magn Reson Imaging **5,** 201, 1987.
27. Feldkamp, L.A., Davis, L.C., and Kress, J.W. Practical cone-beam algorithm. J Opt Soc Am **1,** 612, 1984.
28. Hoekstra, J.W., van den Beucken, J.J., Leeuwenburgh, S.C., Meijer, G.J., and Jansen, J.A. Tantalumpentoxide as a radiopacifier in injectable calcium phosphate cements for bone substitution. Tissue Eng Part C Methods **17,** 907, 2011.
29. Chesnick, I.E., Fowler, C.B., Mason, J.T., and Potter, K. Novel mineral contrast agent for magnetic resonance studies of bone implants grown on a chick chorioallantoic membrane. Magn Reson Imaging **29,** 1244, 2011.
30. Wichlas, F., Bail, H.J., Seebauer, C.J., Schilling, R., Pflugmacher, R., Pinkernelle, J., Rump, J., Streitparth, F., and Teichgräber, U.K. Development of a signal-inducing bone cement for magnetic resonance imaging. J Magn Reson Imaging **31,** 636, 2010.
31. Bergin, C.J., Pauly, J.M., and Macovski, A. Lung parenchyma: projection reconstruction MR imaging. Radiology **179,** 777, 1991.
32. Sieber, M.A., Pietsch, H., Walter, J., Haider, W., Frenzel T., and Weinmann, H.J. A preclinical study to investigate the development of nephrogenic systemic fibrosis: a possible role for gadolinium-based contrast media. Invest Radiol **43,** 65, 2008.
33. Runge, V.M., and Wells, J.W. Update: safety, new applications, new MR agents. Top Magn Reson Imaging **7,** 181, 1995.
34. Girard, O.M., Ramirez, R., McCarty, S., and Mattrey, R.F. Toward absolute quantification of iron oxide nanoparticles as well as cell internalized fraction using multiparametric MRI. Contrast Media Mol Imaging **7,** 411, 2012.
35. Srinivas, M., Cruz, L.J., Bonetto, F., Heerschap, A., Figdor, C.G., and de Vries, I.J. Customizable, multi-functional fluorocarbon nanoparticles for quantitative *in vivo* imaging using 19F MRI and optical imaging. Biomaterials **31,** 7070, 2010.
36. Wu, Y., Chesler, D.A., Glimcher, M.J., Garrido, L., Wang, J., Jiang, H.J., and Ackerman, J.L. Multinuclear solid-state three-dimensional MRI of bone and synthetic calcium phosphate. Proc Natl Acad Sci U S A **96,** 1574, 1999.

Address correspondence to:
Arend Heerschap, PhD
Department of Radiology
Radboud University Nijmegen Medical Center
PO Box 9101
6500 HB Nijmegen
The Netherlands

E-mail: a.heerschap@rad.umcn.nl

Received: January 5, 2012
Accepted: August 24, 2012
Online Publication Date: January 18, 2013